The Effects of Baseline Length in Computed Tomography Perfusion of Liver

# The Effects of Baseline Length in Computed Tomography Perfusion of Liver

Silvia Malavasi[a,b], Alessandro Bevilacqua[a,c,*], Giampaolo Gavelli[d], Domenico Barone[d]

[a] *ARCES (Advanced Research Center on Electronic Systems), University of Bologna, Via Toffano 2/2, Bologna, ITALY I40125*
[b] *CIG (Interdepartmental Centre "L. Galvani"), University of Bologna, Via G. Petroni, 26, Bologna, ITALY I40126*
[c] *DISI (Department of Computer Science and Engineering), University of Bologna, Viale Risorgimento, 2, Bologna, ITALY I40136*
[d] *Istituto Scientifico Romagnolo per lo Studio e la Cura dei Tumori (IRST) IRCCS, Meldola (FC), ITALY I47014*

**Abstract**

Objective: Computed Tomography perfusion (CTp) of liver is very attractive for predictive and prognostic purposes, but motion artefacts and radiation dose connected to duration of examinations jeopardize the reproducibility of perfusion values, thwarting CTp daily application in clinics. The goal is showing to what extent these issues can be faced by shortening the CTp unenhanced stage (i.e., the baseline).

Methods: 59 patients with colorectal cancer underwent undelayed hepatic CTp examinations. For each patient, fifteen virtual examinations $E_\tau$ simulating different scan delays $\tau \in [1..15]$ s were achieved from the undelayed original sequence $E_0$. Absolute (AD), percentage (PD) and compound differences ($CD_\tau$) were computed between $E_0$ and each $E_\tau$ for baseline and perfusion values and measured in HU and arbitrary units (a.u.), respectively. Patients were grouped and counted based on the differences achieved.

Results: Maximum perfusion $CD_\tau < 10$ a.u. and baseline $CD_\tau < 7$ HU were achieved. For $\tau \leq 10$ s, maximum perfusion $CD_\tau \in [5,6)$ a.u. was found in one

*Corresponding author

*Email address:* alessandro.bevilacqua@unibo.it, Phone: +390512095409 (Alessandro Bevilacqua)

*URL:* http://cvg.deis.unibo.it (Alessandro Bevilacqua)

patient only as well as maximum baseline $CD_\tau \in [2,3)$ HU. Blood flow (BF), hepatic perfusion index and arterial BF showed the lowest $CD_\tau$, while portal BF and total BF the highest ones. PD is practically always higher than AD.

Conclusion: The approach presented allows clinicians to design the shortest CTp acquisition protocol, selecting the highest delay compliant with the required accuracy for the chosen perfusion parameters, to limit patient's motion and improve image quality.

Significance: A short CTp protocol allows strengthening the reliability of perfusion values, and correctness of clinical outcomes, advancing CTp introduction in the standard clinical practice.
**Key Words:** Blood Flow, Time Concentration Curves, Measurement errors, Baseline, Reproducibility

---

## 1. Introduction

Computed Tomography perfusion (CTp) is a functional imaging technique that has shown to be very useful in several clinical applications [1], including oncology [2, 3]. Indeed, through the repetition of CT acquisitions of the same tissue portion before, during, and after the administration of a iodinated contrast agent [4] it is possible to extract for each voxel the so-called time concentration curves (TCCs), which allow describing tissue hemodynamics. Several kinetic models can be adopted to describe different aspects of tissue physiology [5]. Accordingly, different methods can be employed for CTp parameters computation, whether they consider only the first passage of contrast agent, where the maximum slope is suitable, or recirculation is also addressed, where deconvolution-based approaches using the time attenuation curves (i.e., achieved from TCCs after removing the baseline [6]) are more appropriate. Therefore, depending on the kinetic model selected and the method applied, time concentration and attenuation curves [7] are processed to extract different perfusion parameters exploited for detection, diagnosis, and prognosis of several pathologies [8, 9, 10]. At present, two wide European multicentre liver CTp studies (SARAH [11] and PROSPeCT [12]) exist, aiming at developing predictive and prognostic imaging biomarkers. It is worth noting that with respect to non-ionizing imaging modality such as Dynamic Contrast Enhanced-Magnetic Resonance Imaging, CTp has a high spatial and temporal resolution, a lower cost, it is widely spread, and changes in attenuation are proportional to contrast agent, this making CTp more suitable for quantitative dynamic analyses [13].

Despite its great potential, CTp has met difficulties to yield reliable and reproducible results due to different causes, including motion artefacts [14] and the limited radiation dose delivered to patients for each CT scan (that however cannot be increased because of the high number of CT volumes needed [15]), that are delaying CTp standardization and its consequent introduction in the standard clinical practice. To face motion artefacts, several approaches have been adopted. The first ones aiming at preventing motion by involving patients directly (e.g., asking them to hold their breath during acquisition) are really effective, but suitable only for very short duration acquisition protocols (i.e., at most, during the first-pass) [16, 17]. A second set of approaches works in post-processing, relying on manual or automatic alignments methods [18, 19], although in the literature there is a lack of standard or widely acknowledged registration algorithms [20, 21]. Finally, a third group of recent approaches acts at the methodological level focusing on reliability issues in general, for instance, improving acquisition sampling to prevent the effects of motion [22], quantifying and removing residual artefacts [23, 24], and providing measurements of perfusion reliability [25]. Nonetheless, all these problems are indissolubly related to the data quality issue and, ultimately, to the dose administered to patients. As regards this item, several efforts have been done to find the best trade-off between data quality and radiation dose saving [15]. The two main approaches that have been explored to reduce radiation administered to patients consist in varying the acquisition parameters (e.g., by diminishing tube current and voltage [26, 27]) and in reducing the number of CT volumes acquired (e.g., by increasing the time sampling [28] or by shortening the acquisition time [29]). However, all these techniques inevitably may yield a loss in signal quality or a reduction of temporal resolution, both affecting accuracy of results.

A further challenging strategy is to try tackling both motion and radiation dose issues together, in one time, that is trying shortening the unenhanced portion of the TCCs (namely, the baseline) by introducing a scan delay between contrast agent administration and acquisition beginning, thus favouring breath hold and motion control, accordingly. Since the baseline is the reference signal before contrast agent arrives [30], it has a great importance in CTp imaging (in general, in signal processing [31]). In fact, besides affecting the overall signal fitting, in the methods where the baseline is the background signal used to achieve the time attenuation curves [30], possible baseline's inaccuracies can heavily hinder the overall CTp parameters computation [6]. For this reason, some recent guidelines on liver CTp suggest to

start acquisition even *before* contrast agent injection [4]. For instance, five to ten unenhanced scans are recommended in [32] to ensure the acquisition of enough baseline samples so as to obtain reliable perfusion values. However, since contrast agent takes time to flow from the injection site to the tissue analysed [33], a huge number of unenhanced scans could be unnecessary. Indeed, almost all the hepatic CTp studies reported in the literature adopt varying scan delays, *after* contrast agent injection, according to two main strategies. The most conservative one consists in applying no scan delays at all, this resulting in long acquisition protocols that do ensure TCCs with a long baseline portion, but at patients' comfort and health expenses. An example of such protocol can be found in [34], where CTp results are used as the gold-standard since the absence of scan delay allows obtaining as much accurate CTp results as possible. On the contrary, the second approach consists in introducing high scan delays, adopting a shorter acquisition protocol that permits a better motion control and a substantial radiation dose saving. An example of this choice can be found in [35], where a varying scan delay ranging from 8 s to 10 s allows obtaining a consistent baseline shortening, but with the risk of introducing notable inaccuracies caused by short and length-varying baselines.

While all these approaches rely on heuristic criteria to set the baseline length, the work in [36] is an early attempt to measure the effects of scan delay on perfusion parameters, with the aim of reducing the dose administered to patient. The work provides resuming results regarding the effects of scan delay on perfusion values, but without either discussing the causes of worsening in accuracy or mentioning how many patients are involved.

The main goal of this study is to measure the effects of shortening the unenhanced sequence of CTp liver examinations on baseline, TCCs and perfusion values accuracy, extensively discussing the underlying causes. To this purpose, fifty-nine hepatic CTp studies carried out with no scan delay (whose perfusion results represent a benchmark) are analysed. Stemming from the original acquisitions, several datasets are generated for each patient simulating the usage of acquisition protocols with different scan delays, according to what reported in [36]. Baseline values and different perfusion parameters are calculated for each dataset using the maximum slope method, and the effects of shortening the baseline through scan delays are measured for each patient by using the original sequences as a reference. The results confirm the possibility to introduce a moderate, and sometimes high, delay in CTp examinations without losing clinical information either on baseline or perfusion

values. This allows achieving a very short protocol with possible reduction of motion artefacts and overall improvement of the overall CTp reliability, accordingly, thus promoting its applicability in the clinical practice.

## 2. Materials and methods

### *2.1. Background*

Grounded on the indicator-dilution theory [37], the hepatic tissue can be modelled as a mono-compartmental system [38] and the Fick principle describing the mass conservation law [39] can be applied. In particular, the Fick's principle states that the mass of contrast agent inside tissue $c_T(t)$ depends on the organ's blood flow (BF), and on contrast agent concentration inside the vascular input $c_i(t)$ and the venous output $c_o(t)$ [39], according to (1):

$$dc_T(t)/dt = BF \cdot [c_i(t) - c_o(t)]. \tag{1}$$

Immediately after contrast agent injection, the tracer remains inside tissue. During this period, it is possible to make the assumption of no venous outflow (i.e., $c_o(t)$=0) and write (1) as follows:

$$dc_T(t)/dt = BF \cdot c_i(t). \tag{2}$$

This means that the rate of tracer accumulation inside tissue $c_T(t)$ is maximal when also the concentration of the vascular input $c_i(t)$ is maximal, and (2) can be thus reformulated:

$$\frac{dc_T(t)}{dt}|_{max} = BF \cdot c_i(t)|_{max}. \tag{3}$$

During first-pass, contrast agent arrival is pointed out by changes in tissue attenuation and BF values can be extracted from (3) as the rate between the tissue $c_T(t)$ maximum gradient and input $c_i(t)$ peak, according to (4):

$$BF = \frac{\frac{dc_T(t)}{dt}|_{max}}{c_i(t)|_{max}}. \tag{4}$$

Besides being apt for the short first-pass protocols, the maximum slope method is robust and simple to compute, allows taking into account both a single and a dual vascular input and, as such, it is one of the mostly used methods in the literature [1]. maximum slope also fits well our purposes, since

exploiting only the first data acquired (i.e., up to the enhancement portion of the tissue TCCs) allows achieving the shortest examination as possible, thus emphasizing the effects of baseline length reduction. In addition, maximum slope allows computing five different perfusion parameters that have shown to be useful for clinical purposes: single-input BF, arterial BF (aBF), portal BF (pBF), total BF (tBF) and hepatic perfusion index (HPI). In particular, the single input BF (ml/min/100g) can be calculated through (4) by replacing $c_i(t)$ with the aortic TCC ($c_a(t)$) [40]. On the contrary, when dual input parameters are considered, $c_T(t)$ is split into two portions by the peak instant of the splenic TCC to separately evaluate through (4) the arterial ($c_T^a(t)$) and the portal ($c_T^p(t)$) contributions to tissue vascular circulation due to the aortic and the portal ($c_p(t)$) input, respectively [41]. tBF (ml/min/100g) is finally calculated as the sum of the arterial and the portal contributions to perfusion, according to (5):

$$tBF \ = aBF \ + pBF. \tag{5}$$

Finally, HPI (%) represents the arterial contribution to the hepatic circulation and is computed according to (6):

$$HPI = aBF/tBF. \tag{6}$$

To include analyses of local BF changes in clinical evaluations, the numerical values of perfusion parameters in the region of interest (ROI) are usually coupled to colorimetric maps.

### *2.2. Dataset and acquisition protocol*

This retrospective study was approved by the Institutional Review Board. 59 adult patients (P) with colorectal cancer, but free from liver metastases and chronic hepatic diseases, provided written informed consent and were included in this study. Each patient was instructed to breath shallowly and underwent a hepatic CTp examination carried out using a 64-slice multidetector CT scanner (LightSpeed VCT; GE Healthcare, Milwaukee, WI, USA). After a first unenhanced CT scan used to localize the portal trunk, an axial CTp acquisition was performed on the identified region using fixed tube current (100 mA) and voltage (80 kV), with gantry rotation time of 1 s. 40 ml of iodinated contrast agent (350 mg·I/ml) were injected at 5 ml/s contextually to acquisition beginning (i.e., no delay). 60 scans over a section of 40 mm, representing 8 slices with 5 mm thickness, 5 mm spacing, and 0.49 mm pixel

size, were performed every 1 s for the first 30 s and every 3 s for the subsequent 90 s, finally yielding 480 CT images (512×512 pixel). The image acquisition procedure is resumed in the movie M1 that can be found in the **Supplementary Files**.

*2.3. TCC's extraction and fitting*

Despite the original study was conceived to investigate also the contrast agent equilibrium phase, in the present research we focused our attention on the first-pass phase. Accordingly, the first 42 CT scans (i.e., the first 65 s, roughly corresponding to the arterial first-pass phase) were extracted from each examination not to take advantage from samples not available in a short-time protocol explicitly conceived to analyse only the first-pass phase. In order to extract TCCs on which computing baseline values and perfusion parameters, each CTp examination was first analysed by two experienced radiologists in cine-loop mode and the central slice of each of the first 42 volumes acquired was selected to generate the reference sequence [34, 42, 43]. Four ROIs were drawn in consensus to outline liver tissue, aorta, portal vein, and spleen. Tissue ROI was drawn as large as possible on the first slice of the reference sequence, excluding large vessels and keeping ROI borders far enough from liver margins to prevent partial volume effects [44]. Instead, the remaining three ROIs were outlined on the slices showing aortic, portal, and splenic maximum enhancement to assure the correct computation of perfusion parameters and weaken any problem related to patient motion. In those examinations where portal vein or spleen were not visible due to the narrow field of view adopted, only the single input analysis was carried out. Then, the ROIs outlined were aligned on the other slices of the reference sequence to allow TCCs extraction. In particular, a single mean TCC was obtained for aorta, portal vein, and spleen by averaging their ROIs' density values in each time instant. As far as the tissue is concerned, a first filtering step was applied to improve data quality before TCCs extraction. In particular, preliminary exploratory analyses on tissue motion confirmed that breath was shallow and slow and the maximum displacement found between two consecutive slices was lower than 10 mm. Consequently, in order to filter image noise preserving edges and reduce the effects of motion improving TCCs temporal coherency [45], a 3D 9×9×3 median filter of approximate size of 4.4 mm ×4.4 mm ×1.5 mm was applied on liver tissue. Then, voxel-based TCCs were extracted from the tissue ROI and fitted using the sigmoidal Hill's model, often employed to describe pharmacokinetic of contrast agent

during first-pass phase [22, 46], and reported in (7):

$$\hat{c_T}(t) = E_{\text{MIN}} + (E_{\text{MAX}} - E_{\text{MIN}})\frac{t^\alpha}{(EC_{50} + t)^\alpha} \tag{7}$$

where $E_{min}$ and $E_{max}$ are the TCC's baseline and maximum (saturation) values, respectively, $EC_{50}$ is the time instant of the half-maximum response concentration of the curve and $\alpha$ is the nonlinear parameter mostly affecting signal's slope. Then, a fitting was accomplished on the remaining three parameters through the Interior Point minimization algorithm implemented in the *fmincon* function of Matlab© (MathWorks Inc, Natick, MA, USA). As the cost function $F(\cdot)$, the sum of squared residuals computed between the fitted signal $\hat{c_T}(t)$ and the original TCC $c_T(t)$ in each time instant $i$ was chosen, according to (8):

$$F = \sum_i (c_T(i) - \hat{c_T}(i))^2. \tag{8}$$

The bounds of fitting parameters were adjusted to speed-up the overall processing time and to avoid non-physiological solutions. Accordingly, $E_{min}$ was set to the baseline value found with the algorithm described in [47]. As regards $E_{max}$, to set the lower bound we have not to forget that the Hill equation is a monotonic sigmoidal model conceived to represent only the ascent part of the TCC. For this reason, in order to force fitting not to include HU values belonging to the TCC's washout phase, the lower bound of $E_{max}$ was set to the 90-*th* percentile of each tissue TCC density range (whose maximum value is the TCC's peak). In fact, while lower values clearly include many samples of the descent phase, choosing a higher values selects too a low number of samples in the peak's neighbourhood (or even isolated peaks due to noise), that makes them loosing representativeness. As for EC50, it was left free within its whole physiological range, that is between the end of baseline ($t_B$) [47] and the TCC's peak time. Finally, as far as $\alpha$ is concerned, negative values yield decreasing $\hat{c_T}(t)$, while $0 < \alpha \leq 1$ yields curves without baseline, soon increasing at the first time instant, this being infeasible with our CTp protocol (Sect. 2.2). Accordingly, since $\hat{c_T}(t)$ has a baseline only if $\alpha$>1, we chose 1.1 as the lower bound. As for its upper bound, early analyses carried out to explore the parameter space suggested that setting $\alpha$=15 did not yield any $\alpha$-saturated fitting, and this was confirmed by the post-processing analysis of the ultimate sigmoidal parameter values. It also worth saying that,

as $\alpha$ increases, the changes in TCC' slope rapidly decreases, exponentially, with very low differences between subsequent $\alpha$ values. The starting points were set to the middle range values.

### *2.4. Generation of virtual TCCs*

In order to evaluate the effects of TCCs shortening on baseline values and perfusion results, several datasets with different delays $\tau$ ($E_\tau$) were built for each patient starting from the original acquisitions ($E_0$, with $\tau$=0 s), which were used as the reference ones. In particular, the set of delayed CTp examinations $E_\tau$ was obtained from $E_0$ ones by progressively disregarding the first $i$ CT scans. The maximum number of samples disregarded (i.e., fifteen) was selected to assure the presence of at least one baseline data-point in each TCC, after an automatic analysis of the patients' baseline lengths carried out through the algorithm described in [47]. Being the sampling time equal to 1 s for the first thirty seconds, the number $i$ of CT scans discarded coincides with $\tau$. For instance, to simulate an acquisition protocol with a scan delay of $\tau$=10 s it is necessary to remove the first 10 CT scans from $E_0$. Therefore, for each patient sixteen examinations (one $E_0$ and fifteen $E_\tau$) were associated to as many delayed acquisition protocols. The same datasets were previously used to provide some hints to reduce the administered dose in liver CTp while maintaining diagnostic accuracy [36].

### *2.5. Assessment of results and statistical analyses*

The quality of each examination was determined by calculating the image signal-to-noise ratio (SNR, measured in dB) of each $E_0$, according to (9):

$$\mathrm{SNR} = 20 \cdot \log_{10}(m_L/\sigma_B) \tag{9}$$

where $m_L$ is the mean density value calculated in the liver ROI and $\sigma_B$ is the standard deviation of the slice background. The goodness-of-fit was estimated for each TCC by calculating the mean value $\mu_\epsilon$ of the absolute residuals $\epsilon$ between $c_T(t)$ and $\hat{c_T}(t)$, according to (10):

$$\mu_\epsilon = \frac{1}{M}\sum_{i=1}^{M} |c_T(i) - \hat{c_T}(i)| \tag{10}$$

where $M$ is the number of samples of the TCC considered [23]. For each patient, the voxel-based baseline values and single and dual input perfusion

parameters were computed for $E_0$ and each $E_\tau$ exploiting the maximum slope method. The absolute differences (AD) and the absolute percentage differences (PD) referred to baseline and perfusion values computed on $E_0$ and each $E_\tau$ were calculated and resumed by their median values. Fifteen comparisons (one for each couple ($E_0$, $E_\tau$)) were performed on 59 patients for baseline and BF, and on 48 patients for the four dual-input perfusion parameters (i.e., those for which the dual-input analysis was feasible). It is worth noting that we need introducing a unique "perfusion unit" (p.u.) to enable a comparison between HPI and BF-based parameters, since they have different measurement units. For instance, 5p.u. corresponds to 5% when the measure is referred to HPI or to 5ml/min/100g when it concerns BF, aBF, pBF, or tBF.

The Shapiro-Wilk test (p-value$\leq$0.05) was used to test Gaussianity of the baseline and perfusion median values distributions. The two-tail paired Wilcoxon signed-rank test was performed to evaluate significance of baseline and perfusion variations caused by the scan delays, although it is worth mentioning that a statistically significant difference may not be clinically significant. Accordingly, in order to favour the clinical translation of results, we extended the tests to check to what extent baseline and perfusion AD and PD were significantly different from zero, by testing them against a set of integer Hounsfield Unit (HU) and p.u., respectively, and percentage values. In particular, the one-tail paired Wilcoxon signed-rank test was repeatedly applied to test baseline and perfusion AD values for each couple ($E_0$, $E_\tau$) against integer N HU and p.u., N=[1$\div$20]. The same test was also applied to evaluate integer PD, with N=[1$\div$100] percentage.

In addition, besides analysing AD and PD separately, considering that it may happen that their magnitudes are in inverse relation, as emerged from preliminary analysis, we try proposing for each patient $i$ one significant compound (CD) difference, for each $\tau$, according to (11):

$$\mathrm{CD}_{i,\tau} = \min(\mathrm{AD}^i_\tau, \mathrm{PD}^i_\tau), \forall i \in \mathrm{P} \tag{11}$$

that is, the minimum between percentage and absolute difference.

This arises from considering that same values for AD and PD could have the same clinical importance (for instance, to this purpose AD=5 ml/100g/min and PD=5% are equivalent). In fact, they both are used in the literature, with no indication of which of these methods is preferable, or whether a different magnitude should be considered when using percentage or absolute

differences. As a consequence, we propose one resuming significant difference for each $\tau$ ($CD_\tau$), for baseline and perfusion values, described in (12):

$$CD_\tau = \max_{i \in P}(CD_{i,\tau}) \tag{12}$$

In practice, $CD_\tau$ represents for each $\tau$ the highest compound difference found in all patients, whether it is AD or PD.

All the statistical tests were performed by using IBM® SPSS® Statistics 23.0 (IBM Corp., Armonk, NY, USA), where p-value$\leq$0.05 was considered for statistical significance. The movie M2 in the **Supplementary Files** schematizes and resumes the procedures described in 2.3, 2.4, and 2.5 to extract the original TCCs, generate the virtual datasets associated to different $\tau$'s and to assess the results.

### *2.6. Tables and Graphs for results interpretation*

To help the reader to better interpret the outcomes, besides the mere statistical significance of the absolute and statistical differences, we counted the number of patients for which a given difference is significant, so as to allow computing the prevalence for each variation. In particular, we prepared a set of Tables (3-4, and SI-SX in the **Supplementary Files**) containing even the number of patients showing a maximum variation N-1$\leq$AD<N and N-1$\leq$PD<N for each N>0 value, as $\tau$ varies. These outcomes were summarized through two intuitive graphs (Fig. 5(a) and (b)) pointing out for each delay $\tau$ and perfusion parameter the highest variation found. As regards $CD_\tau$ for baseline and perfusion values, it is represented in two graphs, Fig. 4 and Fig. 8, respectively, were however we keep track of whether AD or PD prevails, using squared or "pointed" bars, respectively.

## 3. Experimental Results

Initially, we compare the outcome of our perfusion parameters' computation method, calculated on the whole sequence $E_0$, with those reported in the literature (section 3.1). After that, we present the variations of baseline and CTp parameters computed with different scan delays $\tau$, analysing their causes (sections 3.2 and 3.3). We then analyse a sample case study 3.4 and, finally, propose some practical hints on how to properly shorten the baseline 3.5.

*3.1. Baseline and perfusion values of the whole sequence*

Median baseline values calculated for each examination $E_0$ are reported in the histogram of Fig. 1. Although global median (62.8 HU) and mean

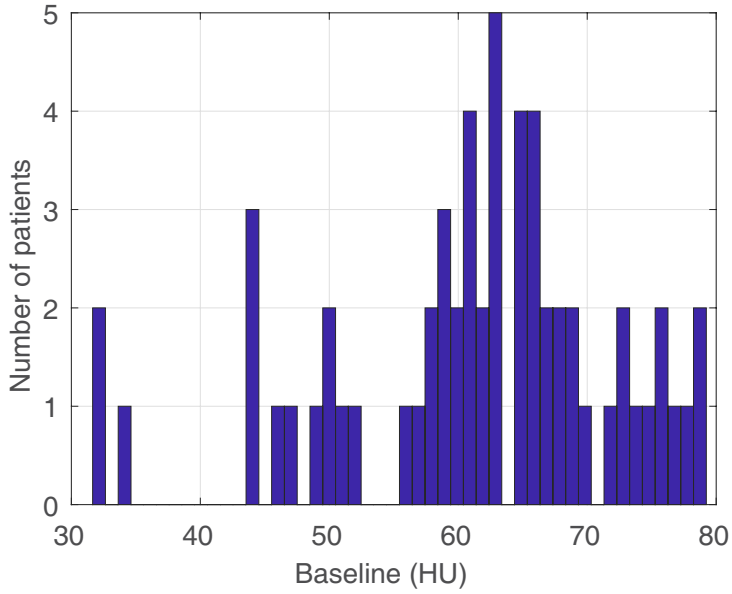


Figure 1: Histogram of median $E_0$ baseline values of all patients.

(61.2 HU) values differs, leaving the three leftmost outliers out of consideration, the distribution is Gaussian, with a standard deviation of 11.2 HU. These values are compliant with those of normal liver density measured with unenhanced CT scans in [48], that reported comparable global mean and standard deviation (58.8±10.8 HU), collected from healthy liver of even 3357 patients with colorectal cancer.

As regards the distributions of the median perfusion parameters, only HPI is Gaussian (p-value=0.8), while BF, aBF, pBF, tBF show p-values≤0.03. However, to enable a comparison with the other works, Table 1 only shows mean, standard deviation, and range of the median perfusion parameters values computed on $E_0$ of each patient, since these are the only parameters available in these papers. These perfusion values were compared with those calculated on normal liver tissue in patients with hepatocellular carcinoma [49, 34], or metastases from colorectal cancer [50], since no works address healthy liver in colorectal cancer patients. In general, we see that all standard deviations reported are wider than ours, probably due to the lower

| Perfusion parameter | $\mu \pm \sigma$ | Range |
|---|---|---|
| BF (ml/min/100g) | 36.4 ± 13.0 | 16.6–74.5 |
| aBF (ml/min/100g) | 24.4 ± 12.9 | 5.1–74.5 |
| pBF (ml/min/100g) | 94.4 ± 24.7 | 55.5–151.7 |
| tBF (ml/min/100g) | 119.5 ± 32.4 | 72.4–209.7 |
| HPI (%) | 20.6 ± 7.2 | 4.7–35.5 |

Table 1: Mean ($\mu$), standard deviation ($\sigma$), and range of median BF, aBF, pBF, tBF, and HPI values referring to $E_0$ of each patient are reported.

number of patients and the liver analysed being a healthy portion in the presence of cancer. In fact, our mean and standard deviation of single-input BF are comparable with those reported in [49] (39.6±17.3 p.u.). Similarly, our mean and range value for aBF are compliant with those reported in [50] (24.5 p.u. and [10.4–71.1 p.u.]) as well as our mean and range values for HPI are compatible (24.0 p.u. and [15.0–35.0 p.u.], respectively). Instead, the mean pBF is higher than in [50] (73,6 p.u.), although our range is fully included ([32.3–172.3 p.u.]). Finally, as regards tBF, our mean and standard deviation values are compliant with those reported in [34] (118.3±92.9 p.u.), even though we have a far smaller standard deviation.

### *3.2. The effects of delay $\tau$ on TCCs and baseline*

Fig. 2 shows the boxplots of median baselines' AD (a) and of BF's AD (b) as $\tau$ increases (graphs referred to PD, and to AD of the remaining four perfusion parameters are similar and have not been reported). As expected, baseline values and perfusion parameters accuracy decreases as TCCs shorten. Indeed, by decreasing the number of unenhanced data samples available, the baseline values calculated are less accurate and baseline AD values increase, this altering the time attenuation curves. Besides that, with fewer samples also data fitting worsens, this reducing precision of perfusion parameters, which leads perfusion AD to increase. The monotonic increasing trend of both baseline and perfusion variations as TCCs shorten clearly points out that the baseline values computed on $E_\tau$, and the related perfusion results, gradually move away from their reference values calculated on $E_0$. Furthermore, the increase of the interquartile range of both baseline AD and perfusion AD and PD means that patients' baseline and perfusion values are more and more differently sensible to the lack of samples caused by shortening of

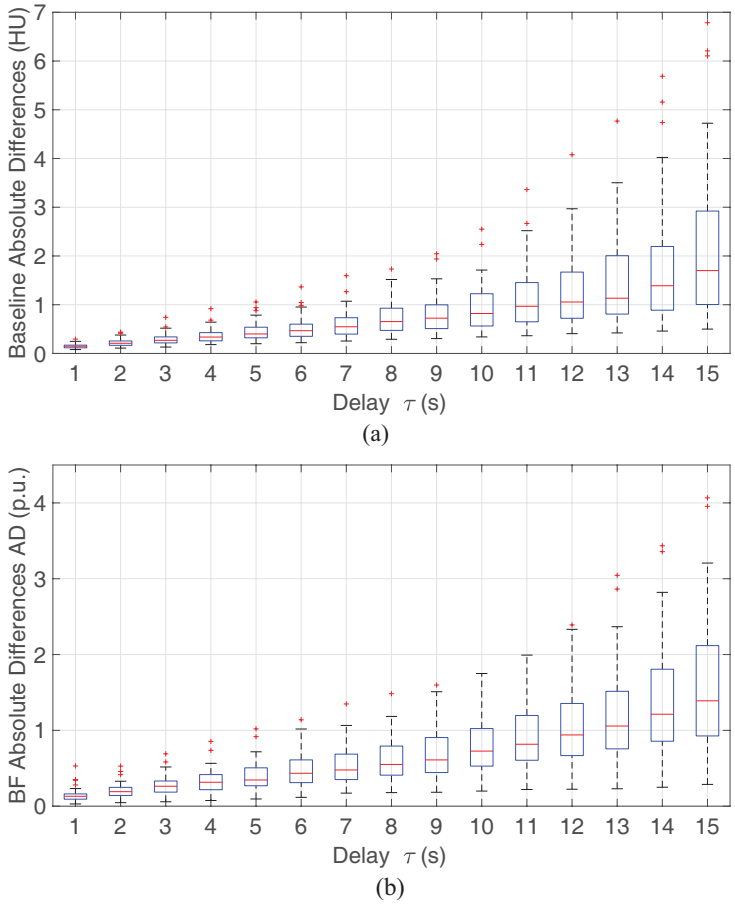


Figure 2: Baseline (a) and BF (b) absolute differences AD achieved for all patients as the baseline is shortened.

the unenhanced portion of TCCs. This mainly depends on the quality of data acquired and on the time taken by contrast agent to reach the liver, which can vary on the basis of patients' physiological factors (e.g., the cardiac output) [33]. In fact, TCCs characterised by higher noise levels or with shorter baselines are more prone to fitting errors and, consequently, to heavier variations of perfusion results. Fig. 3 (a) and (b) deals with TCCs referring to two examinations with a different SNR, where the same scan delay ($\tau$=12 s) causes a similar baseline AD of about 0.5 HU. Despite the same very small variation, this produces very different effects on the final perfusion results of the two examinations. Indeed the TCC in Fig. 3 (a), pertaining to patient

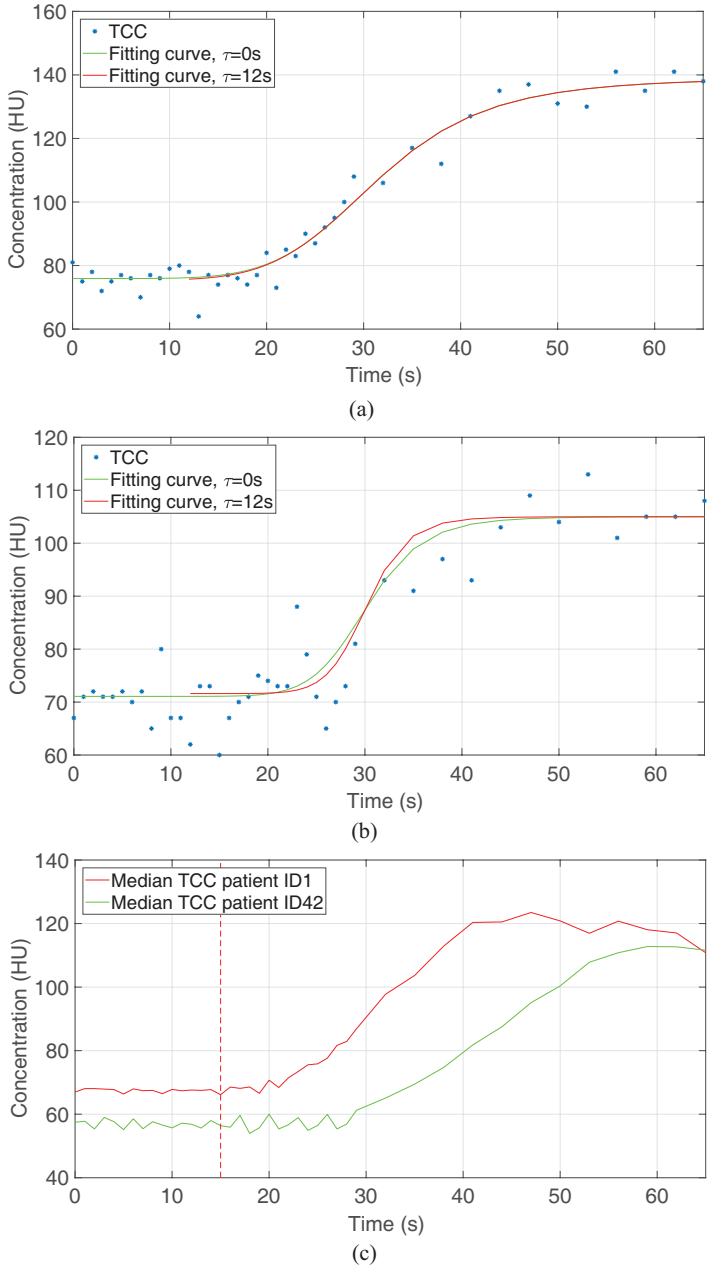


Figure 3: Sampling TCCs and relative fitting curves found in patients ID85 (a) and ID86 (b) considering all the data samples or neglecting the first twelve data points. Median TCCs of patients ID1 (in the red colour) and ID42 (in the green colour) (c).

ID85 (i.e., the one with the highest quality, with SNR=13.4 dB), is characterised by a low temporal noise ($\mu_\epsilon$=3.1 HU). Consequently, the fitting keeps almost unchanged whether considering the whole signal or just part of it and leads to a BF AD of only 0.1 p.u. Differently, the TCC of patient ID86 (SNR=5.3 dB) reported in Fig. 3 (b) is noisier ($\mu_\epsilon$=4.1 HU) and the fitting error caused by the lack of 12 samples leads to BF AD of 18.0 p.u. Fig. 3 (c) shows the effects of different contrast agent arrival on two mean TCCs of patients ID1 (in red) and ID42 (in green), with a similar SNR (8.3 dB and 7.5 dB, respectively). As one can see, whereas in patient ID1 contrast agent takes on average about 19 s to arrive inside tissue, in patient ID42 it needs 27 s. This means that when introducing a scan delay of 15 s (highlighted by the red vertical dashed line in Fig. 3 (c)), in patient ID1 there are on average only 5 unenhanced samples available, whereas in patient ID42 there are 8 more samples that definitely contribute to achieve more precise baseline values and more accurate perfusion results, accordingly. In fact, both median baseline and perfusion variations found in patient ID1 after excluding the first 15 samples (i.e., $\tau$=15 s) from the analysis are higher than those found in patient ID42 (Table 2).

| AD | ID1 | ID42 |
|---|---|---|
| Baseline (HU) | 1.0 | 0.5 |
| BF (p.u.) | 1.0 | 0.4 |
| aBF (p.u.) | 1.1 | 0.8 |
| pBF (p.u.) | 4.2 | 1.0 |
| tBF (p.u.) | 3.1 | 0.2 |
| HPI (p.u.) | 0.9 | 0.8 |

Table 2: Median baseline and perfusion parameters' absolute differences AD calculated between $E_0$ and $E_\tau$ (with $\tau$=15 s) for patients ID1 and ID42 characterized by very different contrast agent's arrival times (i.e., 19s and 27s, respectively).

### *3.3. Baseline and perfusion values as $\tau$ varies*

The increase of baseline AD as TCCs shorten has been confirmed by the statistical analysis. In particular, baseline AD have shown in Table 3 to be significantly lower than 1 HU and 2 HU in all patients for scan delays up to 4 s and 9 s, respectively. In addition, as $\tau$ increases from 10 on, only one, or at most two patients at a time, are responsible for worsening AD's. Fig. 4

| $\tau$ \N | 1 | 2 | 3 | 4 | 5 | 6 | 7 | 8 |
|---|---|---|---|---|---|---|---|---|
| 1 | 59 | 0 | 0 | 0 | 0 | 0 | 0 | 0 |
| 2 | 59 | 0 | 0 | 0 | 0 | 0 | 0 | 0 |
| 3 | 59 | 0 | 0 | 0 | 0 | 0 | 0 | 0 |
| 4 | 59 | 0 | 0 | 0 | 0 | 0 | 0 | 0 |
| 5 | 58 | 1 | 0 | 0 | 0 | 0 | 0 | 0 |
| 6 | 58 | 1 | 0 | 0 | 0 | 0 | 0 | 0 |
| 7 | 57 | 2 | 0 | 0 | 0 | 0 | 0 | 0 |
| 8 | 52 | 7 | 0 | 0 | 0 | 0 | 0 | 0 |
| 9 | 51 | 8 | 0 | 0 | 0 | 0 | 0 | 0 |
| 10 | 46 | 11 | 2 | 0 | 0 | 0 | 0 | 0 |
| 11 | 42 | 13 | 3 | 1 | 0 | 0 | 0 | 0 |
| 12 | 37 | 15 | 5 | 1 | 1 | 0 | 0 | 0 |
| 13 | 34 | 15 | 5 | 4 | 1 | 0 | 0 | 0 |
| 14 | 28 | 17 | 7 | 3 | 2 | 2 | 0 | 0 |
| 15 | 23 | 17 | 6 | 5 | 4 | 2 | 2 | 0 |

Table 3: The number of patients showing a baseline absolute difference AD significantly lower than N as the delay $\tau$ varies. On the right side of the red line, for given delays there are no patients with such significant variations.

shows baseline's $CD_\tau$, where CD is equal to AD for all $\tau$'s, pointing out that

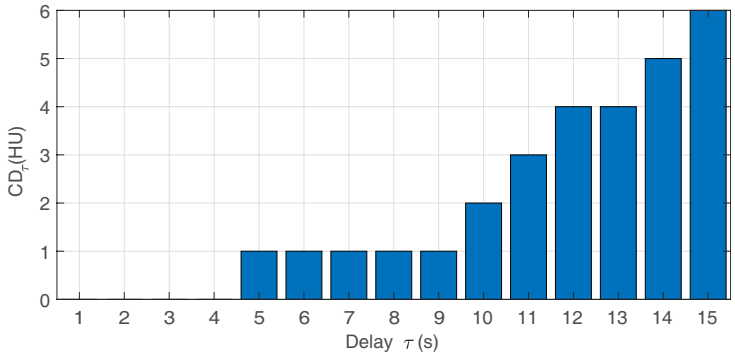


Figure 4: Summary of the statistical test for compound differences $CD_\tau$ carried out on baseline. Here, $CD_\tau$=$AD_\tau$, for all $\tau$'s.

AD is always lower than PD.

Table 4 reports the results of statistical tests (AD) carried out on BF.

| $\tau$ \N | 1 | 2 | 3 | 4 | 5 | 6 |
|---|---|---|---|---|---|---|
| 1 | 59 | 0 | 0 | 0 | 0 | 0 |
| 2 | 59 | 0 | 0 | 0 | 0 | 0 |
| 3 | 59 | 0 | 0 | 0 | 0 | 0 |
| 4 | 59 | 0 | 0 | 0 | 0 | 0 |
| 5 | 59 | 0 | 0 | 0 | 0 | 0 |
| 6 | 59 | 0 | 0 | 0 | 0 | 0 |
| 7 | 59 | 0 | 0 | 0 | 0 | 0 |
| 8 | 57 | 2 | 0 | 0 | 0 | 0 |
| 9 | 55 | 4 | 0 | 0 | 0 | 0 |
| 10 | 52 | 7 | 0 | 0 | 0 | 0 |
| 11 | 48 | 10 | 1 | 0 | 0 | 0 |
| 12 | 42 | 14 | 3 | 0 | 0 | 0 |
| 13 | 41 | 15 | 2 | 1 | 0 | 0 |
| 14 | 30 | 21 | 6 | 2 | 0 | 0 |
| 15 | 27 | 18 | 10 | 2 | 2 | 0 |

Table 4: The number of patients showing a BF absolute difference AD significantly lower than N as the delay $\tau$ varies. On the right side of the red line, for given delays there are no patients with such significant variations.

For instance, the row referring to $\tau$=12 s points out that by neglecting the first twelve samples, fourteen patients (i.e., about 24%) show significant BF AD of 1 p.u., three more patients (i.e., about the 5%) reports BF AD of 2 p.u., while in the remaining 42 examinations (i.e., about the 71%) there are no changes. Therefore, this means that by shortening the baseline by 12 samples, BF variations up to 2 ml/min/100g are expected in nearly 30% of patients. In general, just at a first glance it is possible to see how the number of patients with higher perfusion variations increases as TCCs shorten. This growth is not linear with the delay and becomes faster at given $\tau$'s, for the different parameters considered. For instance, whereas for $\tau$=1 s there are no patients showing significant BF AD, for $\tau$=8 s the number of patients with significant BF AD of at least 1 p.u. increases to 2 (i.e., 3%) and for $\tau$=15 s it even jumps to 32 (i.e., 54%). The same interpretation holds for Tables SI–SX reported in the **Supplementary Files**, referring to the statistical tests on AD and PD of the different perfusion parameters.

The results of patient-based statistical analysis carried out on each per-

fusion parameter can be resumed by the graphs of Fig. 5. Here, the highest

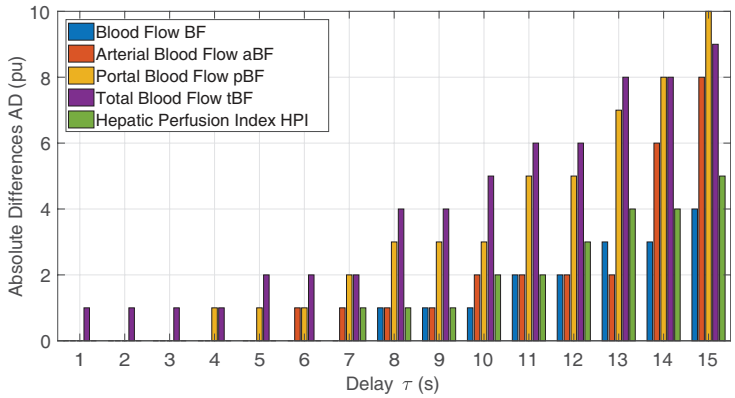


(a)

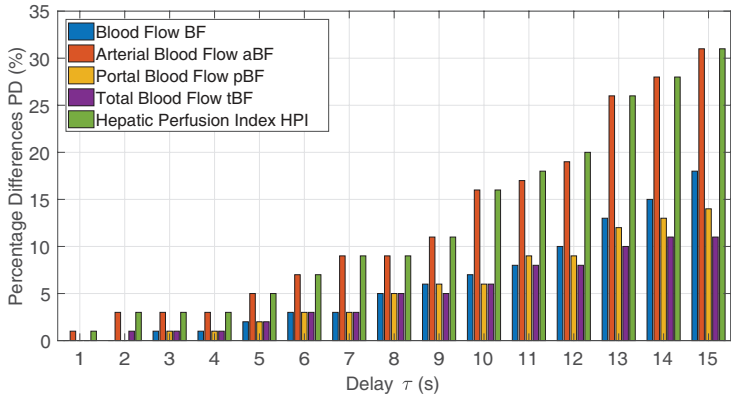


(b)

Figure 5: Summary of the statistical test results carried out on BF, aBF, pBF, tBF, and HPI. For each delay $\tau$, the highest statistically significant median absolute difference AD (a) and percentage difference PD (b) found in at least one patient are reported.

statistically significant AD (Fig. 5 (a)) and PD (Fig. 5 (b)) found in at least one patient for each perfusion parameter and $\tau$ are reported. For instance, assuming that a scan delay of 11 s has been introduced, there is at least one patient that has shown BF, aBF and HPI AD of 2 p.u. and pBF and tBF AD of 5 and 6 p.u., respectively. In agreement with the results previously discussed, the resuming graphs of Fig. 5 clearly show that a gradual increase of both perfusion AD and PD occurs as shorter acquisition protocols are considered. Indeed, by focusing attention on bars of the same colour, it is possible to see the monotonic increasing trend of perfusion parameters

AD and PD. As it can be seen in Fig. 5 (a), BF and HPI are the parameters showing the lowest significant AD. Indeed, independently from the scan delay considered, these two parameters show significant AD of maximum 4 p.u. and 5 p.u., respectively. Differently, aBF AD values up to $\tau$=13 s are in good agreement with those of BF and HPI, whereas for longer scan delays they rapidly increase up to 8 p.u. This is supposedly due to aBF being computed on the first portion of the TCC, where data samples missed for high $\tau$ value makes fitting more prone to inaccuracies. On the contrary, pBF and tBF are the parameters showing the highest significant AD for all the $\tau$ considered. However, as shown in Table 1, pBF and tBF are also the parameters characterised by the highest absolute perfusion values and the lowest PD (Fig. 5 (b)), accordingly. Conversely, aBF and HPI are characterised by the highest PD (Fig. 5 (b)), having the lowest absolute perfusion values (Table 1).

### *3.4. A sample case study*

To better understand the practical effects of introducing different scan delays on perfusion results, an example of colorimetric maps computed on different $E_\tau$ is shown in Fig. 6. In particular, the colorimetric maps of pBF (i.e., the parameter having the highest significant AD) of a sample patient ID69 for $\tau$=0 s, 5 s, 10 s, and 15 s are shown. As one can see, at first sight the four maps are characterised by practically the same perfusion pattern. However, the median AD and PD values reported in Table 5 for each scan

| $\tau$ (s) | AD (p.u.) | PD (%) |
|---|---|---|
| 5 | 1.5 | 1.7 |
| 10 | 2.9 | 3.3 |
| 15 | 5.7 | 6.3 |

Table 5: pBF median absolute (AD) and percentage difference (PD) values of patient ID69 calculated between $E_0$ and three different $E_\tau$ (with delay $\tau$=5 s, 10 s and 15 s).

delay considered point out that perfusion results vary more and more by shortening baseline length.

Furthermore, through a thorough analysis of the colorimetric maps of Fig. 6 it is possible to notice that the hepatic tissue follows two main behaviours. In the rightmost ROI, perfusion values do not change noticeably even though long scan delay are introduced. Indeed, median pBF val-

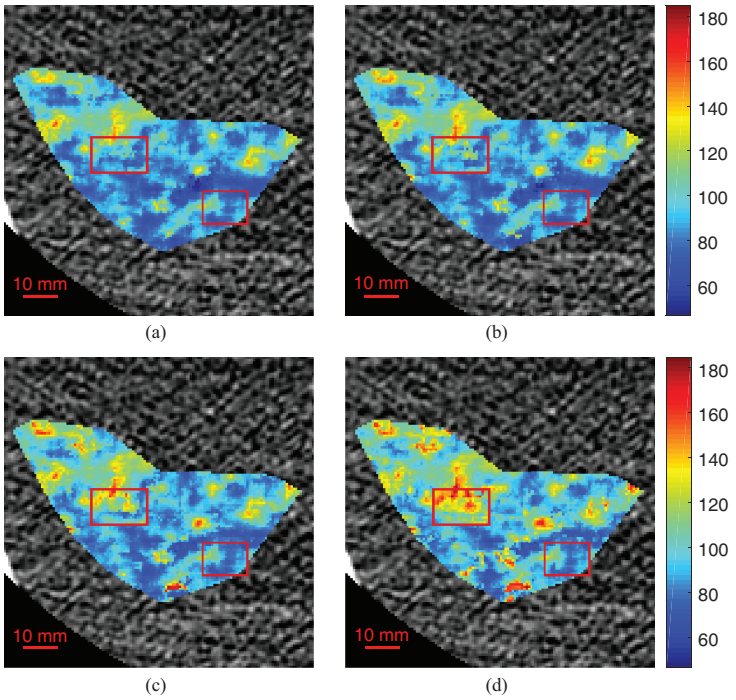


Figure 6: pBF (ml/min/100g) colorimetric maps of patient ID69 calculated on $E_0$ (a) and $E_\tau$ with $\tau$=5 s (b), 10 s (c), and 15 s (d). The red rectangular ROIs point out two tissue regions showing different behaviours.

ues in this region varies from 81.7 ml/min/100g (in $E_0$) to 81.1, 81.7, and 83.6 ml/min/100g as $\tau$ increases to 5 s, 10 s, and 15 s, respectively. The highest AD and PD are found for $\tau$=15 s and are so small (i.e., on average, AD=1.9 ml/min/100g and PD=2.3%) that are practically unnoticeable to the naked eye. On the contrary, the tissue highlighted in the leftmost rectangular ROI shows higher perfusion variations that can be easily noted, especially for longer scan delays. Indeed, while median pBF values obtained for $E_0$ (i.e., 89.5 ml/min/100g) and $\tau$=5 s (i.e., 91.8 ml/min/100g) are similar, strong variations are observed when scan delay $\tau$ is set to 10 s (i.e., 102.4 ml/min/100g) and 15 s (i.e., 120.6 ml/min/100g). In this case, pBF PD of about 14% and 33% have been observed for $\tau$=10 s and 15 s, respectively and can be easily detected even to the naked eye.

The main reason why regions of healthy tissue quite close with one another can have such different behaviours is related to liver physiology. Indeed, in patients with healthy liver, blood arriving from the hepatic artery

and the portal vein takes on average 18 s and 13 s, respectively to transit through the organ [51]. As a consequence, the tissue regions perfused first have a shorter baseline than those characterised by longer transit times. Accordingly, for longer scan delays some TCCs are expected to preserve a long unenhanced portion whereas some others to be characterised by few, or even one, baseline samples. This is what happens in the two TCCs reported in Fig. 7, taken from the rightmost (a) and the leftmost (b) ROIs of Fig. 6. In particular, when a scan delay of 15 s is applied, the TCC in Fig. 7 (a)

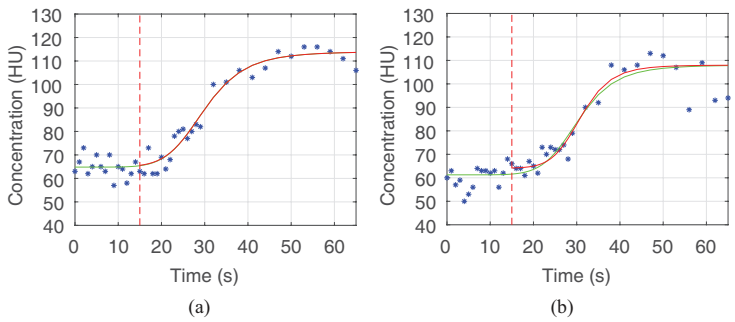


Figure 7: Sample TCCs extracted from the rightmost (a) and the leftmost (b) ROIs drawn in Fig. 6. The fitted curve obtained for $\tau$=0 s (in the green colour) and $\tau$=15 s (in the red colour) are also reported. The red vertical line highlights baseline portion that is excluded from the analysis when adopting $\tau$=15 s.

keeps several unenhanced points (i.e., seven). This allows computing an accurate baseline value (AD=0.2 HU) and obtaining a good fitting that leads to practically identical perfusion results (pBF AD=0.3 ml/min/100g). On the contrary, for $\tau$=15 s the TCC in Fig. 7 (b) is characterised by fewer unenhanced samples (i.e., four), this leading to a baseline AD of 2.9 HU and to different fitting curves, with noticeable consequences on perfusion results (pBF AD=15.6 ml/min/100g).

### *3.5. Choosing a baseline: practical hints*

The delay is chosen with the purpose of having at one's disposal a baseline long enough to compute reliable CTp parameters, where the length is represented by the time needed by contrast agent to reach the body site to be analysed and deduced by physiological knowledge. In addition, it widely varies from voxel to voxel, yet more when the tissue being analysed is tumour. Therefore, it is only possible to deal with baseline shortening with

respect to the expected time, whose knowledge has been refined by the practice of clinical studies, while it could be much harder to fix in advance a given length.

After choosing the perfusion parameters of interest, to select the scan delay in a new acquisition protocol, AD and PD should be taken into account, together with the percentage of patients showing significant perfusion AD and PD. For instance, supposing that in the CTp study design statistician and clinicians agreed that perfusion variations up to 10% can be accepted, only scan delays lower than 9 s should be taken into account. However, with $\tau$=9 s, aBF and HPI PD of 11% correspond to a maximum AD of 1 p.u. that have been observed only in about 8% and 10% of patients, respectively. Therefore, even though a scan delay of 9 s apparently would not be advisable because it leads to PD higher than 10%, the AD introduced are so small and so infrequent that these perfusion variations could not have any clinical relevance and the selection of shorter acquisition protocols should be reconsidered. For this reason, in the graph of Fig. 8 we proposed the

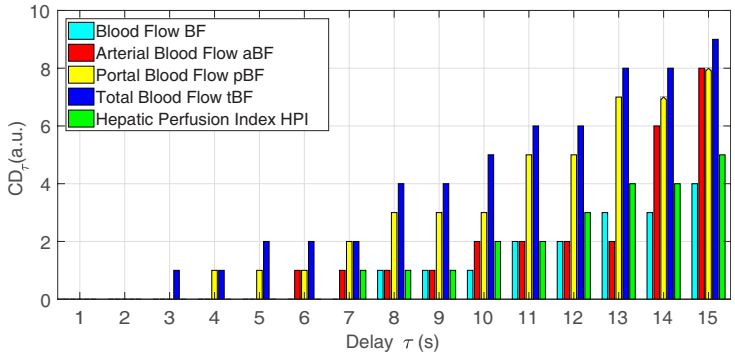


Figure 8: Compound differences CD$_\tau$ computed on BF (cyan), aBF (red), pBF (yellow), tBF (blue), and HPI (green).

compound difference CD (see Sect. 2.6), resuming both AD and PD. As one can see, it is always AD<PD, except for pBF with $\tau \geq 14$ s and tBF with $\tau \leq 2$ s (where PD<1). If this outcome (i.e., AD<PD) could be taken for granted for low perfusion values, it is quite unexpected for high-value perfusion parameters. The main outcome is that, being N equal and standing the above-mentioned exceptions, percentage changes are greater, that is, AD is always more sensitive than PD. This is an important result which should prompt the use of the AD to look for safer statistical significance. Finally,

one more factor to be taken into account in the selection of the best $\tau$ is which are the parameters of interest. Indeed, for instance, assuming that $CD_\tau$<3 p.u. are allowed, a scan delay of 7 s should be chosen if all the perfusion parameters need to be calculated, but it can be increased to 11 s if only BF, aBF, and HPI are of interest.

To highlight the relevance of our study, we take two sample recent CTp liver studies into consideration, the first being too conservative [34], while the second too less [52]. In fact, the choice of the authors in [34] to start image acquisition at the same time of contrast agent injection does not improve perfusion results accuracy, but only administrates unnecessary radiation dose and increases patients' discomfort. On the contrary, the usage of longer scan delays can introduce a degree of perfusion inaccuracy that could jeopardise clinical outcomes, as it happens in [52]. This study, aiming at comparing maximum slope perfusion results achieved using two different approaches to separate hepatic arterial and portal contributions, relies on an 8 s scan delay acquisition protocol. Here, the authors consider as being significant an average pBF AD of 2.2 ml/min/100g between the two strategies. However, besides the two different approaches, also the inaccuracy introduced by neglecting the first eight samples of the TCCs is probably the cause of that pBF variations. In fact, from the graphs of Fig. 5 we see that a delay of 8 s can cause significant pBF AD of 3 ml/min/100g. Moreover, our experiments show that acquiring two more samples (i.e., 6 s delay) would be enough to reduce pBF AD to 1 ml/min/100g, making those results more reliable.

## 4. Conclusion

Motion artefacts and limited radiation dose per CT scan deliverable to patient are the two main causes thwarting CTp reproducibility in oncology and delaying its application in the daily clinical practice. Several works shorten the unenhanced stage of the signal to cope with these issues, assuming that this does not affect perfusion parameters. This is the first work where the effects of shortening the baseline by delay, on perfusion parameters and baseline values, are investigated and measured, to check whether this is feasible without jeopardizing clinical information. This study proved that in liver this is possible while shortening the unenhanced CTp stage up to at least 11 s, depending on the parameters of interest, since we found that the accuracy changes moderately for the baseline values, while decreases unevenly for the different CTp parameters. Moreover, we believe that the awareness of the ef-

fects of baseline shortening on different stages of CTp computation together with the knowledge of extent and prevalence of accuracy variations of both baseline and perfusion values are indispensable tools for selecting the most proper baseline length and achieving more reliable results. A further consideration regards the overall duration of the CTp examination. Using maximum slope to compute the perfusion values, this study provides an approach to work with the shortest CTp protocol as possible. First, this supports the adoption of breath-hold protocols, strongly reducing the effects on motion artefacts. Second, it gives the possibility of either reducing the administered dose, favouring the numerousness of CTp examinations, or keeping it constant by increasing X-ray tube acquisition parameters for each CT scan, thus enhancing image quality, and TCC signal accordingly. In both cases, this improves the reproducibility of CTp analyses, and together with the other findings, advances CTp to its adoption in the standard clinics.

## Authors' contribution

**Silvia Malavasi:** Writing – original draft, Methodology, investigation, Software, Formal analysis **Alessandro Bevilacqua:** Supervision, Methodology, Writing – review & editing, Formal analysis **Giampaolo Gavelli:** Validation **Domenico Barone:** Data curation, Validation.

## Acknowledgement

We would like to thank Prof. Valérie Vilgrain of the Department of Radiology of the Academic Beaujon Hospital for providing us with the data of the Project PIXEL, one of the widest European multicentre study on liver CTp. The PIXEL study was funded by a grant from Programme Hospitalier de Recherche Clinique - PHRC 2007 n°AOM07228, France and sponsored by Assistance-Publique Hôpitaux de Paris (APHP).

## References

[1] N. Kartalis, K. Brehmer, and L. Loizou, "Multi-detector CT: Liver protocol and recent developments," *Eur. J. Radiol.*, vol. 97, pp. 101–109, Dec. 2017.

[2] W. M. Thaiss, A. W. Sauter, M. Bongers, M. Horger, and K. Nikolaou, "Clinical applications for dual energy CT versus dynamic contrast enhanced CT in oncology," *Eur. J. Radiol.*, vol. 84, no. 12, pp. 2368–2379, Dec. 2015.

[3] H. Kim, C. M. Park, J. M. Goo, J. E. Wildberger, and H. U. Kauczor, "Quantitative computed tomography imaging biomarkers in the diagnosis and management of lung cancer," *Invest. Radiol.*, vol. 50, no. 9, pp. 571–583, Sep. 2015.

[4] S. Seyyedi *et al.*, "Low-dose CTp of the liver using reconstruction of difference," *IEEE Trans. Radiat. Plasma Med. Sci.*, vol. 2, no. 3, pp. 205–214, May 2018.

[5] G. S. Ioannidis, T. G. Maris, K. Nikiforaki, A. Karantanas, and K. Marias, "Investigating the correlation of Ktrans with semi-quantitative MRI parameters towards more robust and reproducible perfusion imaging biomarkers in three cancer types," *IEEE J. Biomed. Health Inform.*, Dec. 2018. DOI: 10.1109/JBHI.2018.2888979.

[6] A. B. Gill *et al.*, "A semi-automatic method for the extraction of the portal venous input function in quantitative dynamic contrast-enhanced CT of the liver," *Br. J. Radiol.*, vol. 90, no. 1075, pp. 20160875, Jun. 2017.

[7] S. Turco, W. Hessel, and M. Mischi, "Mathematical models of contrast transport kinetics for cancer diagnostic imaging: a review," *IEEE Rev. Biomed. Eng.*, vol. 9, pp. 121–147, Jun. 2016.

[8] J. M. Hudson *et al.*, "The prognostic and predictive value of vascular response parameters measured by dynamic contrast-enhanced-CT,-MRI and-US in patients with metastatic renal cell carcinoma receiving sunitinib," *Eur. Radiol.*, vol. 28, no. 6, pp. 2281–2290, Jun. 2018.

[9] C. Bendinelli *et al.*, "Perfusion abnormalities are frequently detected by early CTp and predict unfavourable outcome following severe traumatic brain injury," *World J.Surg.*, vol. 41, no. 10, pp. 2512–2520, Oct. 2017.

[10] W. M. Thaiss *et al.*, "Quantification of hemodynamic changes in chronic liver disease: correlation of perfusion-CT data with histopathologic staging of fibrosis," *Acad. Radiol.*, vol. 26, no. 9, pp. 1174–1180, Sep. 2019.

[11] V. Vilgrain *et al.*, "Efficacy and safety of selective internal radiotherapy with yttrium-90 resin microspheres compared with sorafenib in locally advanced and inoperable hepatocellular carcinoma (SARAH): an open-label randomised controlled phase 3 trial," *Lancet Oncol.*, vol. 18, no. 12, pp. 1624–1636, Dec. 2017.

[12] V. Goh, "Information services division scotland. cancer clinical trials service-PROSPECT," 2015. [Online]. Available: http://www.isdscotland.org/Products-and-Services/Cancer-Clinical-Trials-Service/PROSPeCT.asp

[13] M. Ronot *et al.*, "CT and MR perfusion techniques to assess diffuse liver disease," *Abdom. Radiol.*, pp. 1–11, Nov. 2019

[14] L. L. Chu *et al.*, "CTp imaging of lung cancer: benefit of motion correction for blood flow estimates," *Eur. Radiol.*, vol. 28, no. 12, pp. 5069–5075, Dec. 2018.

[15] H. Yabuuchi *et al.*, "Clinical application of radiation dose reduction for head and neck CT." European journal of radiology," *Eur. J. Radiol.*, vol. 107, pp. 209–215, Oct. 2018.

[16] E. Bretas *et al.*, "Is liver perfusion CT reproducible? A study on intra- and interobserver agreement of normal hepatic haemodynamic parameters obtained with two different software packages," *Br. J. Radiol.*, vol. 90, no. 1078, pp. 20170214, Sep. 2017.

[17] D. V. Sahani, N. S. Holalkere, P. R. Mueller, and A. X. Zhu, "Advanced hepatocellular carcinoma: CTp of liver and tumor tissue–initial experience," *Radiology*, vol. 243, no. 3, pp. 736–743, Jun. 2007.

[18] S. Skornitzke *et al.*, "Qualitative and quantitative evaluation of rigid and deformable motion correction algorithms using dual-energy CT images in view of application to CTp measurements in abdominal organs affected by breathing motion," *Br. J. Radiol.*, vol. 88, no. 1046, pp. 20140683, Jan. 2015.

[19] W. R. Crum, T. Hartkens, and D. L. G. Hill, "Non-rigid image registration: theory and practice," *Br. J. Radiol.*, vol. 77, no. suppl_2, pp. S140–S153, Jan. 2004.

[20] A. Hatzidakis *et al.*, "Perfusion-CT analysis for assessment of hepatocellular carcinoma lesions: diagnostic value of different perfusion maps," *Acta Radiol.*, Aug. 2018. DOI: 10.1177/0284185118791200.

[21] V. Granata *et al.*, "Diagnostic accuracy of magnetic resonance, computed tomography and contrast enhanced ultrasound in radiological multimodality assessment of peribiliary liver metastases," *PloS one*, vol. 12, no. 6, pp. e0179951, Jun. 2017.

[22] A. Gibaldi, D. Barone, G. Gavelli, S. Malavasi, and A. Bevilacqua, "Effects of guided random sampling of TCCs on blood flow values in CT perfusion studies of lung tumors," *Acad. Radiol.*, vol. 22, no. 1, pp. 58–69, Jan. 2015.

[23] A. Bevilacqua, D. Barone, S. Malavasi, and G. Gavelli, "Quantitative assessment of effects of motion compensation for liver and lung tumors in CT perfusion," *Acad. Radiol.*, vol. 21, no. 11, pp. 1416–1626, Nov. 2014.

[24] A. Bevilacqua, D. Barone, S. Malavasi, and G. Gavelli, "Automatic detection of misleading blood flow values in CT perfusion studies of lung cancer," *Biomed. Signal Process. Control*, vol. 26, pp. 109–116, Apr. 2016.

[25] A. Bevilacqua, D. Barone, S. Baiocco, and G. Gavelli, "A novel approach for semi-quantitative assessment of reliability of blood flow values in DCE-CT perfusion," *Biomed. Signal Process. Control*, vol. 31, pp. 257–264, Jan. 2017.

[26] Y. Nakamura *et al.*, "Hepatocellular carcinoma treated with sorafenib: arterial tumor perfusion in dynamic contrast-enhanced CT as early imaging biomarkers for survival," *Eur. J. Radiol.*, vol. 98, pp. 41–49, Jan. 2018.

[27] H. P. Marquez *et al.*, "CTp for early response evaluation of radiofrequency ablation of focal liver lesions: first experience," *Cardiovasc. Interv. Radiol.*, vol. 40, no. 1, pp. 90–98, Jan. 2017.

[28] J. C. Ramirez-Giraldo *et al.*, "Evaluation of strategies to reduce radiation dose in perfusion CT imaging using a reproducible biologic phantom," *Am. J. Roentgenol.*, vol. 200, no. 6, pp. W621–W627, Jun. 2013.

[29] C. S. Ng *et al.*, "Metastases to the liver from neuroendocrine tumors: effect of duration of scan acquisition on CTp values," *Radiology*, vol. 269, no. 3, pp. 758–767, Dec. 2013.

[30] E. Klotz *et al.*, "Technical prerequisites and imaging protocols for CTp imaging in oncology," *Eur. J. Radiol.*, vol. 84, no. 12, pp. 2359–2367, Dec. 2015.

[31] A. Gogolou, T. Tsandilas, T. Palpanas, and A. Bezerianos, "Comparing similarity perception in time series visualizations," *IEEE Trans. Vis. Comput. Graph.*, vol. 25, no. 1, pp. 523–533, Jan. 2019.

[32] C. A. Cuenod and D. Balvay, "Perfusion and vascular permeability: basic concepts and measurement in DCE-CT and DCE-MRI," *Diagn. Interv. Imag.*, vol. 94, no. 12, pp. 1187–1204, Dec. 2013.

[33] K. T. Bae, "Intravenous contrast medium administration and scan timing at CT: considerations and approaches," *Radiology*, vol. 256, no. 1, pp. 32–61, Jul. 2010.

[34] S. Mulé *et al.*, "Can dual-energy CT replace perfusion CT for the functional evaluation of advanced hepatocellular carcinoma?," *Eur. Radiol.*, vol. 28, no. 5, pp. 1977–1985, May 2018.

[35] T. Jiang, A. Kambadakone, N. M. Kulkarni, A. X. Zhu, and D. V. Sahani, "Monitoring response to antiangiogenic treatment and predicting outcomes in advanced hepatocellular carcinoma using image biomarkers, CTp, tumor density, and tumor size (RECIST)," *Invest. Radiol.*, vol. 47, no. 1, pp. 11–17, Jan. 2012.

[36] A. Bevilacqua, S. Malavasi, V. Vilgrain, "Liver CTp: which is the relevant delay that reduces radiation dose and maintains diagnostic accuracy?," *Eur. Radiol.*, May 2019. DOI: 10.1007/s00330-019-06259-9.

[37] G. Brix, J. Griebel, F. Kiessling, and F. Wenz, "Tracer kinetic modelling of tumour angiogenesis based on dynamic contrast-enhanced CT and MRI measurements," *Eur. J. Nucl. Med. Mol. Imaging*, vol. 37, no. 1, pp. 30–51, Aug. 2010.

[38] R. Materne *et al.*, "Non-invasive quantification of liver perfusion with dynamic computed tomography and a dual-input one-compartmental model," *Clin. Sci.*, vol. 99, no. 6, pp. 517–525, Nov. 2000.

[39] T.-Y. Lee, "Functional CT: physiological models," *Trends Biotechnol.*, vol. 20, no. 8, pp. S3–S10, Aug. 2002.

[40] K. A. Miles, M. P. Hayball, and A. K. Dixon, "Functional images of hepatic perfusion obtained with dynamic CT," *Radiology*, vol. 188, no. 2, pp. 405–411, Aug. 1993.

[41] T. Kanda *et al.*, "CT hepatic perfusion measurement: comparison of three analytic methods," *Eur. J. Radiol.*, vol. 81, no. 9, pp. 2075–2079, Sep. 2012.

[42] S.Gordic *et al.*, "Correlation between dual-energy and perfusion CT in patients with hepatocellular carcinoma," *Radiology*, vol. 280, no. 1, pp. 78–87, Jan. 2016.

[43] K. Hayano, N. M. Kulkarni, D. G. Duda, R. S. Heist, and D. V. Sahani, "Exploration of imaging biomarkers for predicting survival of patients with advanced non–small cell lung cancer treated with antiangiogenic chemotherapy," *Am. J. Roentgenol.*, vol. 206, no. 5, pp. 987–993, May 2016.

[44] C. S. Ng *et al.*, "CTp in normal liver and liver metastases from neuroendocrine tumors treated with targeted antivascular agents," *Abdom. Radiol.*, vol. 43, no. 7, pp. 1661–1669, Jul. 2018.

[45] G. Treece, "The bitonic filter: linear filtering in an edge-preserving morphological framework," *IEEE Trans. Image Process.*, vol. 25, no. 11, pp. 5199–5211, Nov. 2016.

[46] S. Goutelle *et al.*, "The Hill equation: a review of its capabilities in pharmacological modelling," *Fundam. Clin. Pharmacol.*, vol. 22, no. 6, pp. 633–648, Nov. 2008.

[47] A. Bevilacqua and S. Malavasi, "A novel algorithm to detect the baseline value of a time signal in Dynamic Contrast Enhanced-Computed Tomography," in Proc. of the IEEE International Symposium on Circuits and Systems, Florence, 2018, pp. 1–4.

[48] C. J. Boyce *et al.*, "Hepatic steatosis (fatty liver disease) in asymptomatic adults identified by unenhanced low-dose CT," *Am. J. Roentgenol.*, vol. 194, no. 3, pp. 623–628, Mar. 2010.

[49] E. Frampas *et al.*, "Advanced Hepatocellular Carcinoma: early evaluation of response to targeted therapy and prognostic value of Perfusion CT and Dynamic Contrast Enhanced-Ultrasound," *Eur. J. Radiol.*, vol. 82, no. 5, pp. e205–e211, May 2013.

[50] M. R. Meijerink *et al.*, "Perfusion CT and US of colorectal cancer liver metastases: a correlative study of two dynamic imaging modalities," *Ultrasound Med. Biol.*, vol. 36, no. 10, pp. 1626–1636, Oct. 2010.

[51] H. Sugimoto, T. Kaneko, M. Hirota, E. Tezel, and A. Nakao, "Earlier hepatic vein transit-time measured by contrast ultrasonography reflects intrahepatic hemodynamic changes accompanying cirrhosis," *J. Hepatol.*, vol. 37, no. 5, pp. 578–583, Nov. 2002.

[52] M. A. Fischer, K. Brehmer, A. Svensson, P. Aspelin, and T. B. Brismar, "Renal versus splenic maximum slope based perfusion CT modelling in patients with portal-hypertension," *Eur. Radiol.*, vol. 26, no. 11, pp. 4030–4036, Nov. 2016.